De-orbiting Timing for Spacecraft in Geostationary Transfer Orbits Exploiting Luni-solar Perturbations

By Yue WANG,[1)] and Pini GURFIL[2)]

[1)] *School of Astronautics, Beihang University, Beijing, China*
[2)] *Faculty of Aerospace Engineering, Technion–Israel Institute of Technology, Haifa, Israel*

(Received March 28th, 2017)

Retired spacecraft and spent launch vehicle upper stages in geostationary transfer orbits (GTOs) threaten operational spacecraft in both low Earth orbits and geostationary orbits. Atmospheric re-entry is the preferred end-of-life disposal strategy for low-perigee GTOs. When natural decay of the GTO is not fast enough, an active de-orbiting maneuver is necessary for lowering the perigee. Because of the eccentricity oscillation caused by luni-solar perturbations, de-orbiting maneuvers performed at different timings will affect the GTO differently. Therefore, finding the best timing for the de-orbiting maneuver can exploit the natural luni-solar perturbations to enhance de-orbiting. In this paper, the timing of a de-orbiting maneuver, which is performed at apogee to lower the perigee, is analyzed for retired spacecraft in GTOs. Through analysis and simulations, we find and verify that the minimum point in the eccentricity oscillation is the best timing for the de-orbiting maneuver. With this optimal timing, luni-solar perturbations can be utilized, and the perigee height of the disposal orbit after maneuver will be the lowest among all disposal orbits with different de-orbiting timings. Because of the highly sensitive dynamics introduced by the solar apsidal resonance, a lower perigee can guarantee faster decays of the semi-major axis and eccentricity, as well as an earlier solar apsidal resonance, but cannot guarantee a shorter orbital lifetime.

Key Words: Geostationary transfer orbits, End-of-life disposal, Atmospheric re-entry, De-orbiting timing, Luni-solar perturbations

1. Introduction

Since geostationary transfer orbits (GTOs) cross regions of low Earth orbits (LEOs) and geostationary orbits (GEOs) with large relative velocities, space debris in GTOs pose threats to operational spacecraft in both of these orbital regions. End-of-life disposal measures are required, therefore, for objects in GTOs, to control the growth of the debris population in this orbital region.

Most GTO objects are spent launch vehicle upper stages used to launch GEO satellites. Besides serving as transfer orbits for GEO satellites, GTOs provide low-cost operational orbits for small satellites, which are launched into GTOs as secondary payloads, such as the SPIRALE GTO satellites,[1)] and also serve as operational orbits for satellites studying space radiation environment, such as US CRRES spacecraft[2)] and Japanese Tsubasa satellite.[3)] In the future, the number of satellites operated in GTOs will increase with the spring up of small satellites, and their end-of-life disposal is of great importance for the space debris mitigation.

Generally, there are two end-of-life disposal strategies for Earth-orbiting satellites: atmospheric re-entry and transfer to a graveyard orbit. Usually, it is not an option to move retired spacecraft or spent upper stages from a low-perigee GTO to a graveyard orbit, since it is fuel-consuming to raise the low perigee to above the LEO region (>2000km) and, needless to say, also to move the apogee away from the GEO region. However, it is much easier to lower the perigee deeper into the dense atmosphere. Therefore, atmospheric re-entry is the preferred end-of-life disposal strategy for GTOs with a low perigee. Most GTOs have low perigees, and we will focus on such orbits in this paper.

Because of the low perigee and high apogee, GTOs are affected by the interaction of multiple perturbations, including atmospheric drag, Earth's oblateness, and luni-solar perturbations, which render the dynamical evolution highly sensitive to initial conditions and other parameters. There have been many studies on atmospheric re-entry of GTOs, see e.g. work by Wang and Gurfil[4)] for a review. As a result of the interaction of perturbations, the solar apsidal resonance, the 1:1 resonance between the solar motion and the apsidal rotation caused mainly by Earth's oblateness, introduces high sensitivity into the orbital dynamics.[5)] It has been shown that the high sensitivity in the dynamics and the system uncertainties, especially the large intrinsic uncertainty in the atmospheric density, make deterministic prediction of the GTO's atmospheric re-entry impossible. In practice, a statistical approach is required to estimate the orbital lifetime of GTOs.[6,7)]

The high sensitivity of orbital dynamics and large system uncertainties raise barriers to the design of end-of-life disposal measures, which usually requires predicting orbital lifetime. The statistical method is only feasible for evaluating disposal measures in some specific cases, but not feasible for the disposal design, since it will be unacceptably computationally expensive to evaluate all possible cases during the design process. Therefore, simple guidelines, which can relate the changing trend of orbital lifetime to that of orbital elements, will be useful for the design of end-of-life disposal measures.

There has been a simple guideline widely used in the existing end-of-life disposal measures for atmospheric re-entry from GTOs, that is, a lower perigee height can speed up the orbital decay through the denser atmosphere, or, in other words, a lower perigee can increase the probability of atmospheric re-entry within a given time limit. This fact has been shown using statistical studies by Da Costa et al.[8)] and Morand et al.[6)] However, since the dynamics are highly sensitive, the low perigee

may be raised by the solar apsidal resonance, so this simple guideline is only justified in a statistical sense but not in a deterministic one. Nevertheless, due to the highly sensitive nature of GTO dynamics, the compliance of orbital lifetime with space debris regulations is actually a statistical problem.[6,7] Therefore, this simple guideline is good enough for the design of end-of-life disposal measures for atmospheric re-entry.

Both existing disposal strategies for an early atmospheric re-entry from GTOs have adopted the aforementioned guideline, reducing orbital lifetime by lowering the perigee height as much as possible. The first disposal strategy is exploiting natural perturbations, especially luni-solar perturbations, to decay the orbit in a shorter time that is compliant with space debris regulations. The simplest method is to choose a GTO with a lower initial perigee. However, the GEO satellite will need more fuel to reach the final orbit and will also suffer more drag and thermal effects after the release.[9] For a GTO with a given initial perigee height, several studies have tried to figure out the right initial orbital geometry with respect to the Moon and Sun, so that luni-solar perturbations will lower the initial perigee and then reduce orbital lifetime.[6,8,10–12] In the recent paper,[4] the initial orbital orientation, which leads to a low perigee height, and, consequently, a short orbital lifetime in a statistical sense, has been determined.

The second disposal strategy for an early atmospheric re-entry is an active de-orbiting maneuver, including the direct de-orbiting that leads to a direct re-entry to Earth's atmosphere and the indirect de-orbiting that transfers the spacecraft to a disposal orbit allowing an atmospheric re-entry in a shorter time. De-orbiting maneuvers have been performed by upper stages of the Japanese H-II launch vehicle by the "idle mode burn" shortly after the payload separation in a quasi-retrograde direction near the GTO's perigee.[13] Bonaventure et al.[1] have studied de-orbiting maneuvers at apogee for atmospheric re-entry of the SPIRALE GTO satellites. Through global optimization methods, Colombo et al.[14] and Armellin et al.[15] have designed optimal de-orbiting maneuvers for atmospheric re-entry of the INTEGRAL mission. Although the de-orbiting maneuvers studied in these works are performed at different positions in the orbit and along different directions, they all belong to indirect de-orbiting. These de-orbiting maneuvers aim at lowering the perigee as much as possible and then reducing orbital lifetime through the denser atmosphere, but do not aim at a direct re-entry that requires more fuel. As for the direct de-orbiting, it will be performed by new European launch vehicle Ariane 5 ME with the new engine Vinci.*

The straightest and also the most propellant-efficient method to lower the perigee is to perform a retrograde delta-V maneuver at apogee, as performed by the SPIRALE GTO satellites.[1] In this paper, we focus on this de-orbiting method to lower the GTO perigee for an early atmospheric re-entry. Since luni-solar perturbations induce the eccentricity oscillation, the de-orbiting timing is an important issue. De-orbiting maneuvers with the same delta-V but performed at different timings will act on a GTO with different eccentricities, and then will have different de-orbiting effects. By using analysis and simulations, we will find the best active de-orbiting timing, at which natural luni-solar perturbations can be exploited to the most extent, to achieve the lowest perigee with a given delta-V.

* http://www.esa.int/Our_Activities/Launchers/Launch_vehicles/Adapted_Ariane_5_ME

2. Dynamical Modeling and Orbital Behaviors

2.1. Singly-averaged orbital dynamics

The dynamical evolution of GTOs is governed by orbital dynamics subjected to the perturbations of Earth's oblateness, luni-solar gravity, and atmospheric drag. A singularity-free semi-analytical orbital model in terms of Milankovitch elements was previously derived for GTOs.[4] Through the single averaging process, short-period terms associated with the motion on the GTO are eliminated and the effect of atmospheric drag assumes a simple analytical form. The singly-averaged orbital model allows a multi-orbit time step and the computational speed is improved. In the following, we give a brief description of this model, which will be adopted in this paper.

The Milankovitch elements contains two orthogonal vectors: the orbital angular momentum vector $\boldsymbol{H}$ with the magnitude $\sqrt{\mu a(1-e^2)}$, normal to the orbital plane, and the Laplace vector $\boldsymbol{b} = \mu \boldsymbol{e}$, pointing towards perigee, where μ is the gravitational constant of Earth, a is the semi-major axis, and $\boldsymbol{e}$ is the eccentricity vector. These two vectors can be written in terms of the position $\boldsymbol{r}$ and velocity $\boldsymbol{v}$ as

$$\boldsymbol{H} = \boldsymbol{r}^{\times}\boldsymbol{v}, \boldsymbol{e} = \frac{1}{\mu}\boldsymbol{v}^{\times}\boldsymbol{r}^{\times}\boldsymbol{v} - \frac{\boldsymbol{r}}{r}, \tag{1}$$

where $\boldsymbol{r}^{\times}\boldsymbol{v} = \boldsymbol{r} \times \boldsymbol{v}$ and $\boldsymbol{v}^{\times}\boldsymbol{r}^{\times}\boldsymbol{v} = \boldsymbol{v} \times (\boldsymbol{r} \times \boldsymbol{v})$.

The singly-averaged dynamics of $\boldsymbol{H}$ and $\boldsymbol{e}$ subjected to the perturbations of Earth's oblateness, luni-solar gravity, and atmospheric drag are given by[4]

$$\begin{aligned}
\dot{\boldsymbol{H}} &= \dot{\boldsymbol{H}}_{J_2} + \dot{\boldsymbol{H}}_S + \dot{\boldsymbol{H}}_M + \dot{\boldsymbol{H}}_{Atm} \\
&= -\frac{3\mu J_2 R_E^2}{2a^3h^5}(\hat{\boldsymbol{p}}\cdot\boldsymbol{h})\hat{\boldsymbol{p}}^{\times}\boldsymbol{h} \\
&+ \frac{3a^2\mu_S}{2d_S^3}\left[5\left(\hat{\boldsymbol{d}}_S\cdot\boldsymbol{e}\right)\boldsymbol{e}^{\times}\hat{\boldsymbol{d}}_S - \left(\hat{\boldsymbol{d}}_S\cdot\boldsymbol{h}\right)\boldsymbol{h}^{\times}\hat{\boldsymbol{d}}_S\right] \\
&+ \frac{3a^2\mu_M}{2d_M^3}\left[5\left(\hat{\boldsymbol{d}}_M\cdot\boldsymbol{e}\right)\boldsymbol{e}^{\times}\hat{\boldsymbol{d}}_M - \left(\hat{\boldsymbol{d}}_M\cdot\boldsymbol{h}\right)\boldsymbol{h}^{\times}\hat{\boldsymbol{d}}_M\right] \\
&- \frac{1}{2}B\sqrt{\frac{\mu\left(1-e^2\right)}{2a\pi z}}\rho_{p_0}\exp\left(\frac{r_{p_0}-r_p}{H_\rho}\right)(1+K_1)\boldsymbol{H},
\end{aligned} \tag{2}$$

$$\begin{aligned}
\dot{\boldsymbol{e}} &= \dot{\boldsymbol{e}}_{J_2} + \dot{\boldsymbol{e}}_S + \dot{\boldsymbol{e}}_M + \dot{\boldsymbol{e}}_{Atm} \\
&= -\frac{3nJ_2R_E^2}{4a^2h^5}\left\{\left[1-\frac{5}{h^2}(\hat{\boldsymbol{p}}\cdot\boldsymbol{h})^2\right]\boldsymbol{h}^{\times} + 2(\hat{\boldsymbol{p}}\cdot\boldsymbol{h})\hat{\boldsymbol{p}}^{\times}\right\}\boldsymbol{e} \\
&+ \frac{3\mu_S}{2nd_S^3}\left[5\left(\hat{\boldsymbol{d}}_S\cdot\boldsymbol{e}\right)\boldsymbol{h}^{\times}\hat{\boldsymbol{d}}_S - \left(\hat{\boldsymbol{d}}_S\cdot\boldsymbol{h}\right)\boldsymbol{e}^{\times}\hat{\boldsymbol{d}}_S - 2\boldsymbol{h}^{\times}\boldsymbol{e}\right] \\
&+ \frac{3\mu_M}{2nd_M^3}\left[5\left(\hat{\boldsymbol{d}}_M\cdot\boldsymbol{e}\right)\boldsymbol{h}^{\times}\hat{\boldsymbol{d}}_M - \left(\hat{\boldsymbol{d}}_M\cdot\boldsymbol{h}\right)\boldsymbol{e}^{\times}\hat{\boldsymbol{d}}_M - 2\boldsymbol{h}^{\times}\boldsymbol{e}\right] \\
&- B\frac{1+e}{a\sqrt{2\pi z}}\rho_{p_0}\exp\left(\frac{r_{p_0}-r_p}{H_\rho}\right)(1+K_2)H\hat{\boldsymbol{e}},
\end{aligned} \tag{3}$$

where R_E is the mean equatorial radius of Earth, $\boldsymbol{h} = \boldsymbol{H}/\sqrt{\mu a}$ is the scaled angular momentum, $n = \sqrt{\mu/a^3}$ is the mean motion, $\hat{\boldsymbol{p}}$ is Earth's spin axis, μ_S and μ_M are gravitational constants of the Sun and Moon, respectively, $\boldsymbol{d}_S$ and $\boldsymbol{d}_M$ are po-

sition vectors of the Sun and Moon relative to Earth, respectively, $B = SC_D/m$ is the object's ballistic coefficient, S/m is the area-to-mass ratio (AMR), C_D is the non-dimensional drag coefficient with a typical value of 2.2, $r_p = a(1-e)$, $z = ae/H_\rho$, H_ρ is the constant scale height in the exponential atmospheric density model $\rho = \rho_{p_0} \exp\left[-\left(r - r_{p_0}\right)/H_\rho\right]$, ρ_{p_0} and r_{p_0} are the atmospheric density and the distance from Earth's center at the initial perigee, respectively, and

$$K_1 = \frac{1+3e^2}{8z(1-e^2)}, K_2 = \frac{3e^2-4e-3}{8z(1-e^2)}. \quad (4)$$

2.2. Orbital behaviors

With a low perigee and a high apogee, the GTO is subjected to a complex interaction of multiple perturbations. The Earth's oblateness causes rotations of orbital plane and apsidal line, but on average keeps the orbital shape almost unchanged. Therefore, it does not affect the orbital decay directly but, has indirect effects through the luni-solar perturbations, as will be shown later. Atmospheric drag reduces the semi-major axis and eccentricity gradually with perigee height nearly unchanged. It strongly depends on the atmospheric density and the perigee height, which oscillates due to the luni-solar perturbations.

Luni-solar perturbations depend on the relative positions of the Moon and Sun with respect to the orbital plane and apsidal line. Combining with Earth's oblateness, luni-solar perturbations induce an oscillation of eccentricity and also an oscillation of perigee height. The oscillation is a superposition of a long period, several years, and two short periods, about 14 days and 180 days (half the orbital periods of the perturbing bodies), respectively. The long-period oscillation is induced by the GTO's periodic apsidal rotation caused mainly by Earth's oblateness, while short-period oscillations are induced by periodic luni-solar motions.[4)]

Here, we give an example of dynamical evolution of a GTO by propagating the averaged orbital model (2)-(3). The GTO has the same initial orbital elements with the standard GTO launched by Ariane 5 from Kourou,[†]

$$i_0 = 6 \text{ deg}, h_{a0} = 35943 \text{ km}, \omega_0 = 178 \text{ deg}, \quad (5)$$

where h_{a0} is the initial apogee height, except that it has a different initial perigee height, $h_{p0} = 600$ km, which is equal to that of the SPIRALE GTO satellites.[1)] The initial right ascension of the ascending node (RAAN) Ω_0 is 140 deg. The AMR of the GTO object S/m is 0.01 m^2/kg. The epoch and time step in the simulation are 1 Jan. 2015 00:00:00 UTC and 10000 seconds, respectively.

Time histories of a, e, and h_p for the GTO are given in Figs. 1-3, respectively. Figure 1 shows that the reduction of the semi-major axis caused by the atmospheric drag is quite small, about 1 km per year, and then the semi-major axis is almost constant before the de-orbiting maneuver. Figures 2 and 3 show significant oscillations of the eccentricity and perigee height caused by the luni-solar perturbations, respectively. Our goal is to choose the best point in time of the eccentricity oscillation, at which to perform the retrograde delta-V maneuver at the GTO's apogee, so that the natural luni-solar perturbations can be utilized to enhance de-orbiting.

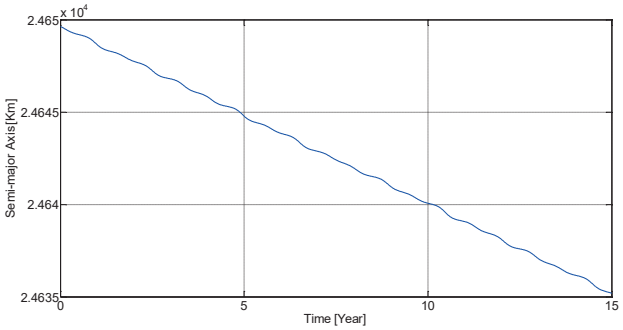

Fig. 1. Time history of a for the GTO without de-orbiting with $h_{p0} = 600$ km.

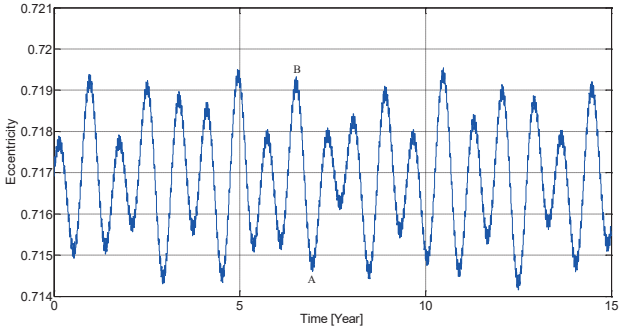

Fig. 2. Time history of e for the GTO without de-orbiting with $h_{p0} = 600$ km.

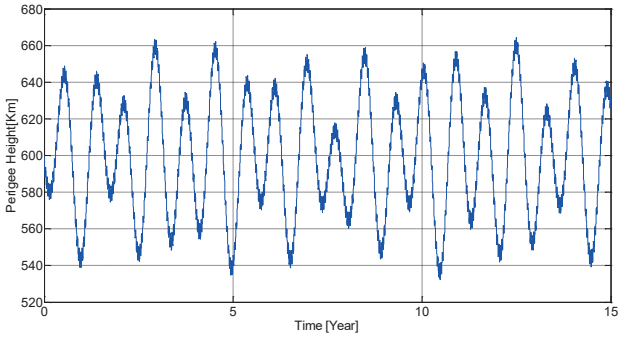

Fig. 3. Time history of h_p for the GTO without de-orbiting with $h_{p0} = 600$ km.

3. Considerations for De-orbiting Timing

The timing of the de-orbiting maneuver at apogee has two aspects: the immediate de-orbiting effect and the longer-term de-orbiting effect. The former can be assessed by Gauss' variational equations, and the latter can be assessed by analyzing the eccentricity oscillation of the disposal orbit after the maneuver.

3.1. Gauss' variational equations

According to the well-known Gauss' variational equations, the change of orbital elements caused by the retrograde delta-V maneuver at apogee are given by

$$\begin{cases} \Delta a = -\dfrac{2}{n}\sqrt{\dfrac{1-e}{1+e}}\Delta V, \\ \Delta e = \dfrac{2}{n}\dfrac{\sqrt{1-e^2}}{a}\Delta V, \end{cases} \quad (6)$$

[†] Ariane 5 User's Manual, Issue 5, Revision 1, July 2011. http://www.arianespace.com/launch-services-ariane5/Ariane5_users_manual_Issue5_July2011.pdf

where the angular orbital elements i, ω, and Ω are unchanged. Therefore, the change of orbital radius at perigee r_p is given by

$$\Delta r_p = \Delta a\,(1-e) - a\Delta e = -\frac{4}{n}\sqrt{\frac{1-e}{1+e}}\Delta V. \qquad (7)$$

According to Eqs. (6)-(7) and the fact that the semi-major axis a is almost constant before the maneuver, with the same ΔV, if the de-orbiting maneuver is performed at the minimum point in the eccentricity oscillation, a and e will be reduced and increased to the most extent, respectively, and, consequently, r_p will be reduced to the most extent.

However, the perigee height of a GTO always oscillates due to the luni-solar perturbations. Therefore, a larger Δr_p cannot guarantee a really lower perigee height after the de-orbiting maneuver. The perigee height oscillations of different disposal orbits, whose de-orbiting maneuvers are performed at different timings, need to be considered also. The perigee height oscillation is actually caused by the eccentricity oscillation. For different disposal orbits, the different perigee height oscillations are mainly attributed to the difference in the eccentricity oscillation, whereas the difference in the semi-major axis has a smaller effect.

Since the orbital orientation with respect to the Moon and Sun is unchanged after the maneuver, the phase of the eccentricity oscillation caused by the luni-solar perturbations is also unchanged. Therefore, if magnitudes of eccentricity oscillations of different disposal orbits are the same, then the minimum point in the eccentricity oscillation mentioned above will be the best timing for the de-orbiting maneuver. This result is true only from the aspect of immediate de-orbiting effect. However, because different eccentricities will lead to different magnitudes of luni-solar perturbations, these disposal orbits actually will have different magnitudes for the eccentricity oscillation. We will discuss this issue in the following.

3.2. Eccentricity oscillation after the maneuver

Here, we consider two candidate points for the de-orbiting maneuver: a minimum point A and a nearby maximum point B in the eccentricity oscillation, as shown in Fig. 4. Eccentricity oscillations of disposal orbits A and B, whose de-orbiting maneuvers are performed at minimum point A and maximum point B, respectively, are depicted by Figs. 5 and 6, respectively.

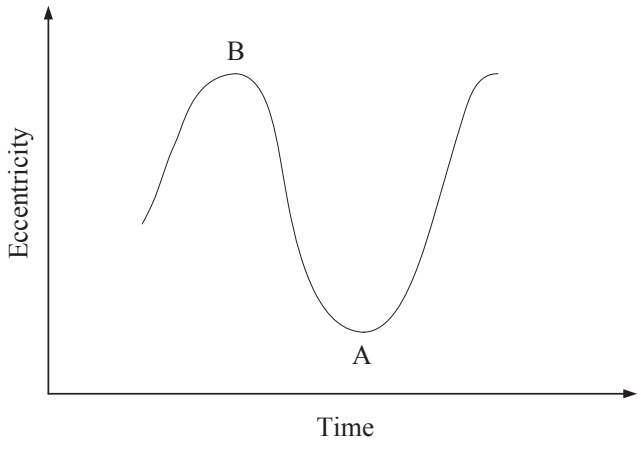

Fig. 4. Minimum point A and maximum point B in the eccentricity oscillation.

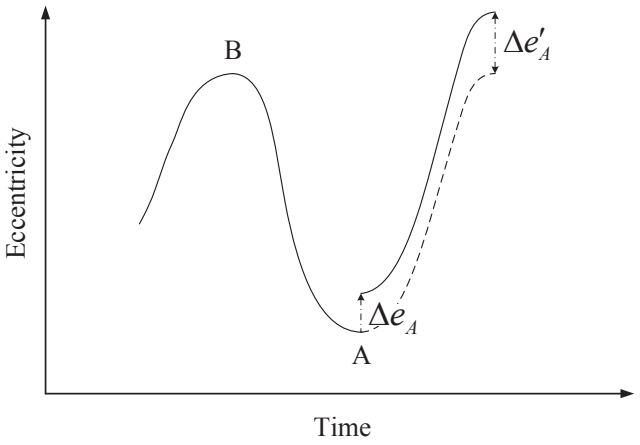

Fig. 5. Eccentricity oscillation of disposal orbit A with de-orbiting at minimum point A.

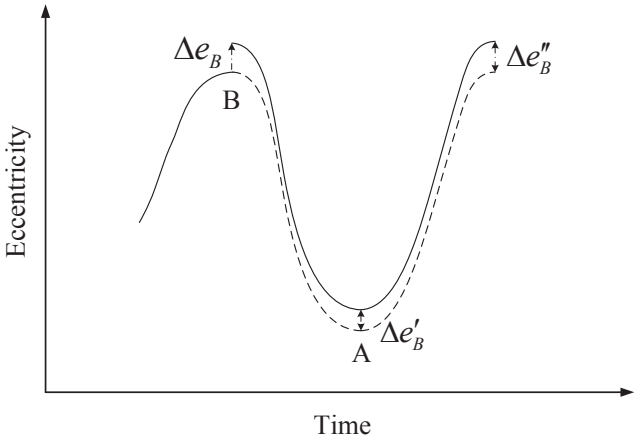

Fig. 6. Eccentricity oscillation of disposal orbit B with de-orbiting at maximum point B.

According to Gauss' variational equation (6) and the fact that the semi-major axis a is almost constant before the maneuver, the changes of eccentricity in Fig. 5 and Fig. 6 are given by

$$\Delta e_A = \frac{2}{n}\frac{\sqrt{1-e_A^2}}{a}\Delta V,\ \Delta e_B = \frac{2}{n}\frac{\sqrt{1-e_B^2}}{a}\Delta V. \qquad (8)$$

Since $e_A < e_B$, we have

$$\Delta e_A > \Delta e_B. \qquad (9)$$

In the same way, we have

$$|\Delta a_A| > |\Delta a_B|\,. \qquad (10)$$

According to the variational equation (3) of $\boldsymbol{e}$, we can see that the magnitude of luni-solar perturbations is larger for a more eccentric orbit. Since $\Delta e_A > 0$, disposal orbit A has a more pronounced eccentricity oscillation than the original orbit. Thus, in Fig. 5, we have

$$\Delta e'_A > \Delta e_A. \qquad (11)$$

Similarly, disposal orbit B also has a more pronounced eccentricity oscillation than the original orbit. Keeping in mind that, unlike point A, point B is the maximum point in the eccentricity oscillation, in Fig. 6, we have

$$\Delta e_B > \Delta e'_B. \qquad (12)$$

According to Eqs. (9)-(12), we have the following inequality

$$\Delta e'_A > \Delta e_A > \Delta e_B > \Delta e'_B. \tag{13}$$

So, we have $\Delta e_A > \Delta e'_B$. Using $\Delta e_A > \Delta e'_B$ and applying the above rule again, we know that, after point A, disposal orbit A has a larger eccentricity oscillation than disposal orbit B, i.e.,

$$\Delta e'_A - \Delta e_A > \Delta e''_B - \Delta e'_B. \tag{14}$$

Then, using $\Delta e_A > \Delta e'_B$ again, we have

$$\Delta e'_A > \Delta e''_B. \tag{15}$$

As stated above, we have following inequalities relating disposal orbits A and B:

$$\begin{cases} |\Delta a_A| > |\Delta a_B|, \\ \Delta e_A > \Delta e'_B, \\ \Delta e'_A > \Delta e''_B, \end{cases} \tag{16}$$

which means that

$$\begin{cases} a_A < a_B, \\ e_{A-\min} > e_{B-\min}, \\ e_{A-\max} > e_{B-\max}. \end{cases} \tag{17}$$

Therefore, we can conclude that from both aspects of immediate and longer-term de-orbiting effects, disposal orbit A has the lowest perigee among all the disposal orbits, whose de-orbiting maneuvers are performed at different points in time of the eccentricity oscillation. Consequently, point A, the minimum point in the eccentricity oscillation, is the best timing for the de-orbiting maneuver at apogee.

4. Numerical Verification

In this section, the above conclusion will be verified by numerical simulations. The simulations are carried out by propagating the averaged orbital model (2)-(3) numerically. We consider the GTO in Section **2.2.** with different initial perigee heights. When the perigee height is lower than 100 km, the spacecraft is regarded burnt and the GTO has decayed.

4.1. $h_{p0} = 600km$

In this simulation example, initial orbital elements and system parameters are all the same as the sample GTO in Section **2.2.**. Assume that the de-orbiting maneuver is to be performed at about the end of the sixth year. To verify the conclusion in Section **3.**, we compare two candidate timings for the de-orbiting maneuver, minimum point A and maximum point B in the eccentricity oscillation in Fig. 2. The magnitude of the de-orbiting maneuver is chosen as $\Delta V = 37$ m/s, the same as the de-orbiting maneuver of the SPIRALE GTO satellites.[1)]

First, we do not take into account the atmospheric drag. The perturbations are Earth's oblateness and luni-solar gravity. Time histories of a, e, and h_p for the original GTO, and disposal orbits A and B without atmospheric drag, are given in Figs. 7-9, respectively.

It can be seen that the semi-major axis of disposal orbit A is about 1.8 km smaller than that of disposal orbit B, as shown in the zoomed lower half of Fig. 7. It can also be seen that disposal orbit A has a larger eccentricity and a lower perigee than disposal orbit B, as shown in Fig. 8 and Fig. 9, respectively.

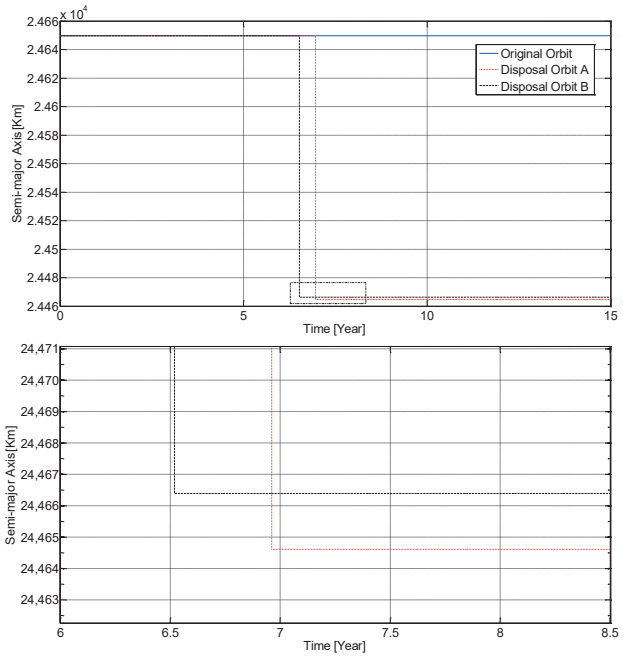

Fig. 7. Time history of a for the original and disposal orbits without atmospheric drag with $h_{p0} = 600$ km.

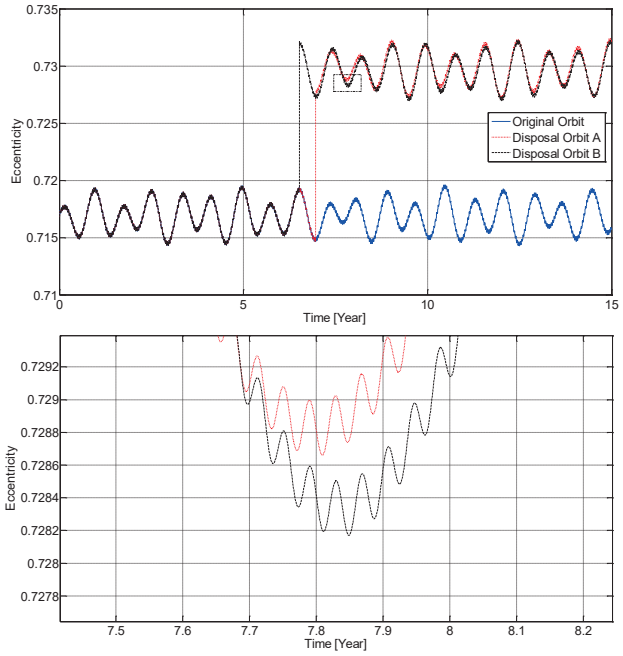

Fig. 8. Time history of e for the original and disposal orbits without atmospheric drag with $h_{p0} = 600$ km.

The maximum difference between minimum perigee heights of disposal orbits A and B is as large as 8 km, as shown in the zoomed lower half of Fig. 9. Therefore, the conclusion in Section **3.** that the minimum point in the eccentricity oscillation is the best timing for the de-orbiting maneuver has been verified.

Next, we take into account atmospheric drag to see the effects of the different perigee heights of disposal orbits on their orbital evolution and lifetime. Time histories of a, e, and h_p for the original GTO, and disposal orbits A and B with full perturbations are given in Figs. 10-12, respectively.

Due to decaying effects, the orbital evolution with full perturbations is totally different from that without atmospheric drag,

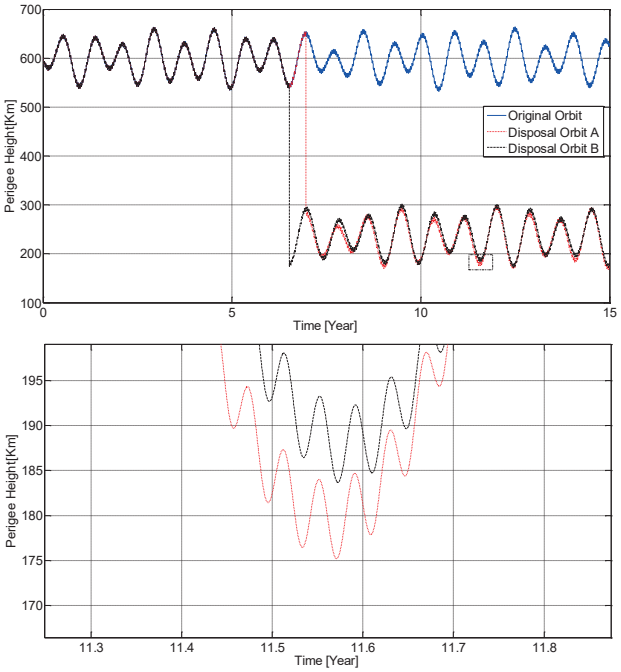

Fig. 9. Time history of h_p for the original and disposal orbits without atmospheric drag with h_{p0} = 600 km.

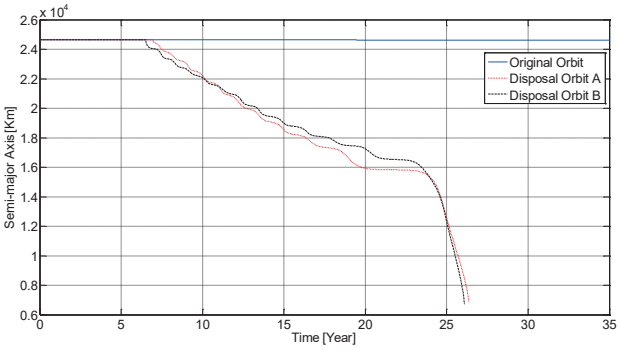

Fig. 10. Time history of a for the original and disposal orbits with h_{p0} = 600 km.

but the lower perigee height of disposal orbit A in the absence of atmospheric drag is retained in the full perturbations model, as shown in Fig. 12. Consequently, the decay rates of a and e of disposal orbit A are larger than that of disposal orbit B, as shown in Fig. 10 and Fig. 11, and then disposal orbit A reaches the condition of solar apsidal resonance about 3 years earlier than disposal orbit B, as shown in Fig. 12.

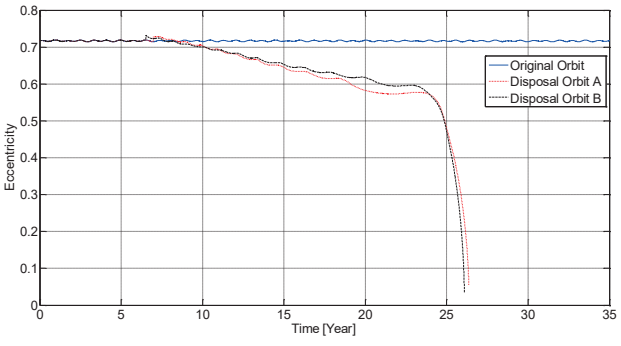

Fig. 11. Time history of e for the original and disposal orbits with h_{p0} = 600 km.

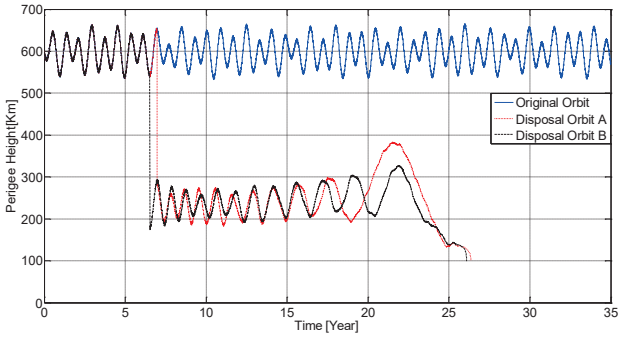

Fig. 12. Time history of h_p for the original and disposal orbits with h_{p0} = 600 km.

However, disposal orbits A and B have different kinds of solar apsidal resonances: the perigee of disposal orbit A is raised by solar gravity to a high altitude, whereas the perigee of disposal orbit B is lowered by solar gravity continuously. As a result, disposal orbit A re-enters Earth's atmosphere almost at the same time as disposal orbit B, but its de-orbiting maneuver is about half a year later than that of disposal orbit B, showing a small advantage in orbital lifetime; but one should keep in mind that it is impossible to predict or manage which kind of solar apsidal resonance will be encountered by the GTO, and the orbital evolution with different kinds of resonances can be totally different.[5] Therefore, as stated in Section **1.**, the solar apsidal resonance is difficult to consider in end-of-life disposal measures for atmospheric re-entry from GTOs. The goal of end-of-life disposal measures is just to achieve a low perigee, without considering the final orbital lifetime directly. A low perigee can speed up the orbital decay, guarantee an earlier solar apsidal resonance, and increase the probability of atmospheric re-entry within a given time limit.[6,8] The compliance of GTO orbital lifetime with space debris regulations is actually a statistical problem.

4.2. $h_{p0} = 800km$

To further verify the conclusion, we consider another simulation example, in which the initial orbital elements and system parameters are the same as in Section **2.2.** except a higher initial perigee h_{p0} = 800 km.

Assume that we want to perform the de-orbiting maneuver circa the seventh year. As in the first example, we also compare two candidate timings for the de-orbiting maneuver, minimum point A and maximum point B in the eccentricity oscillation in Fig. 13. The magnitude of the de-orbiting maneuver is chosen as ΔV = 54 m/s, under the effect of which the perigee height will be reduced to about 200 km.

Time histories of a, e, and h_p for the original GTO, and disposal orbits A and B without atmospheric drag are given in Figs. 14-16, respectively. Similar results to the first example are obtained. The semi-major axis of disposal orbit A is about 2.6 km smaller than that of disposal orbit B, as shown in the zoomed lower half of Fig. 14. Disposal orbit A has a larger eccentricity and a lower perigee. The maximum difference between their minimum perigee heights is as large as 12 km, as shown in the zoomed lower half of Fig. 16.

Next, we take into account atmospheric drag to see the effects of different perigee heights on the orbital evolution and lifetime. Time histories of a, e, and h_p for the original GTO, and disposal

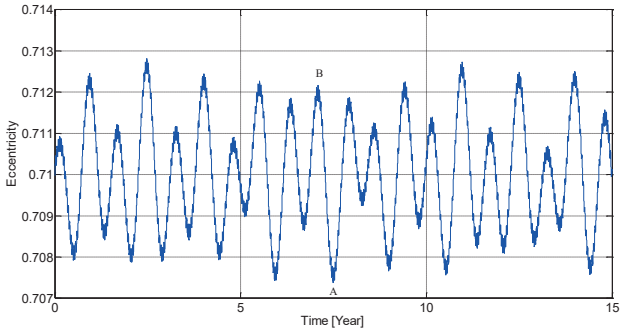

Fig. 13. Time history of e for the GTO without de-orbiting with h_{p0} = 800 km.

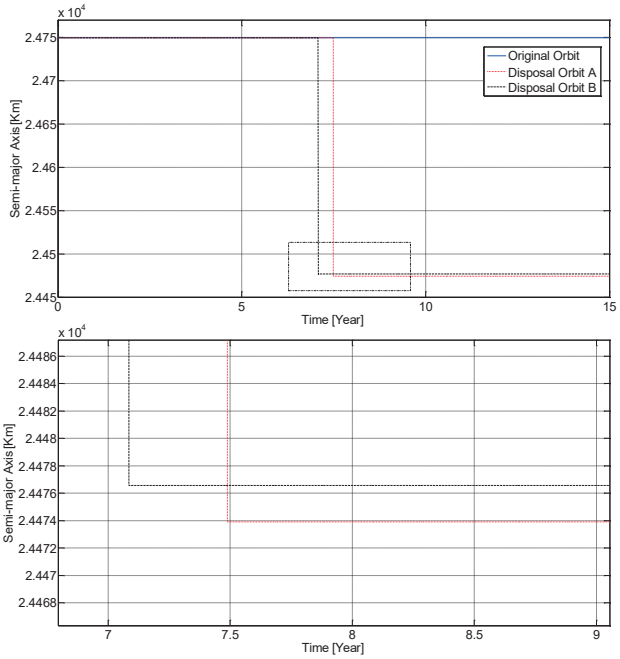

Fig. 14. Time history of a for the original and disposal orbits without atmospheric drag with h_{p0} = 800 km.

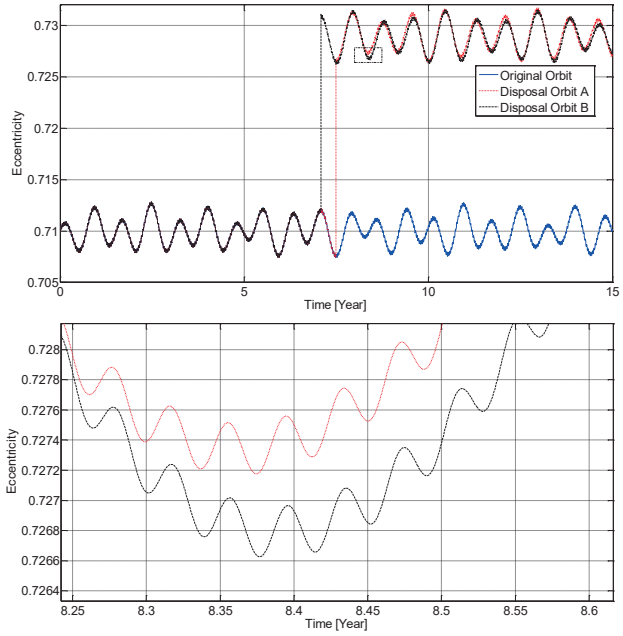

Fig. 15. Time history of e for the original and disposal orbits without atmospheric drag with h_{p0} = 800 km.

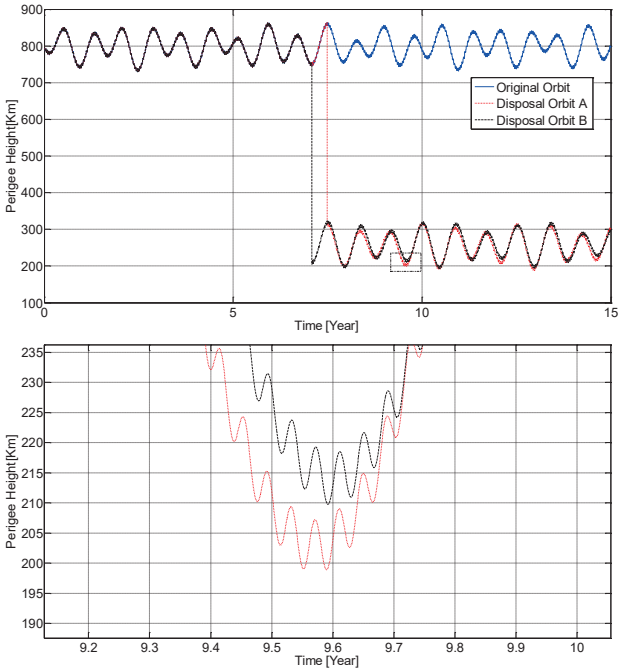

Fig. 16. Time history of h_p for the original and disposal orbits without atmospheric drag with h_{p0} = 800 km.

orbits A and B with full perturbations are given in Figs. 17-19, respectively.

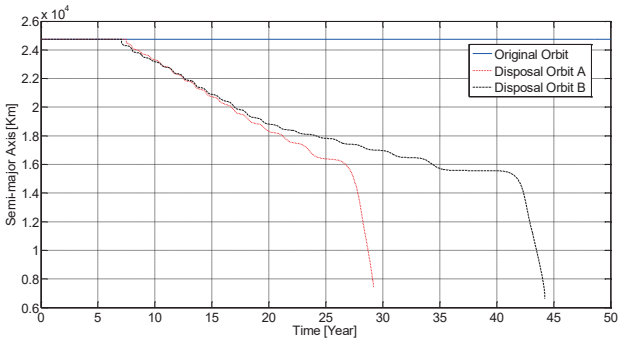

Fig. 17. Time history of a for the original and disposal orbits with h_{p0} = 800 km.

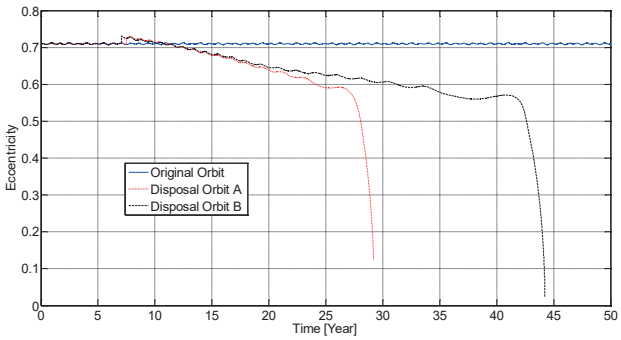

Fig. 18. Time history of e for the original and disposal orbits with h_{p0} = 800 km.

It is seen that the lower perigee height of disposal orbit A in the absence of atmospheric drag is retained in the full perturbations model and, consequently, the decay rates of a and e of disposal orbit A are much larger than that of disposal orbit B. As a result, disposal orbit A reaches the condition of solar apsidal resonance about 10 years earlier than disposal orbit B, as

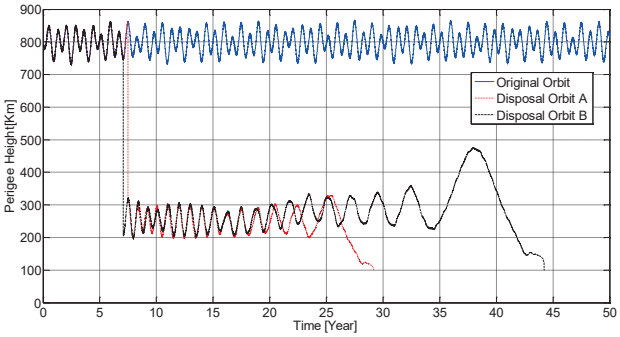

Fig. 19. Time history of h_p for the original and disposal orbits with h_{p0} = 800 km.

shown in Fig. 19. The conclusion in Section **3.** has thus been verified in this example, as well.

Compared with the first example, the advantage of disposal orbit A is more evident for the larger GTO in this example. This can be attributed to the more significant luni-solar perturbations for a larger GTO, which are utilized by performing the de-orbiting maneuver at point A.

Unlike the first example, during the solar apsidal resonance in this example, the perigee of disposal orbit A is lowered by solar gravity continuously, whereas the perigee of disposal orbit B was raised by solar gravity to a high altitude. As a result, disposal orbit A re-enters Earth's atmosphere about 15 years earlier than disposal orbit B, showing clear advantages in orbital lifetime. However, here one should keep in mind that the goal of end-of-life disposal measures is to achieve a low perigee for the disposal orbit, not a shorter orbital lifetime, which is impossible to predict accurately due to the solar apsidal resonance.

5. Conclusions

Through analysis and simulations, it has been found and verified that, for GTOs, the minimum point in the eccentricity oscillation is the best timing for the retrograde active de-orbiting maneuver performed at apogee. When the de-orbiting maneuver is performed at this timing, the luni-solar perturbations can be exploited to the most extent to enhance de-orbiting. Under perturbations of Earth's oblateness and luni-solar gravity, the resulting optimal disposal orbit has the smallest semi-major axis, largest eccentricity, and lowest perigee among all the disposal orbits with different de-orbiting timings.

When the atmospheric drag is also taken into account, the lowest perigee of the optimal disposal orbit is retained. Consequently, the optimal disposal orbit has the largest decay rates of the semi-major axis and eccentricity, and it encounters the solar apsidal resonance earlier than all other disposal orbits. The advantage of the optimal disposal orbit is more dominant for a larger GTO. This is because a larger GTO is subjected to more significant luni-solar perturbations, which is exactly the mechanism utilized by the de-orbiting timing. Since the solar apsidal resonance, which is difficult to predict or manage, may have different effects on the orbital evolution, the optimal disposal orbit with the lowest perigee does not necessarily have the shortest orbital lifetime.

Acknowledgments

This work was supported by the European Research Council Starting Independent Researcher Grant – 278231: Flight Algorithms for Disaggregated Space Architectures (FADER).

References

1) Bonaventure, F., Locoche, S., and Gicquel, A.-H., "De-Orbitation Studies and Operations for SPIRALE GTO Satellites," *The 23rd International Symposium on Space Flight Dynamics*, Pasadena, California, 29 October–2 November, 2012.
2) Johnson, M. H. and Kierein, J., "Combined Release and Radiation Effects Satellite (CRRES): Spacecraft and Mission," *Journal of Spacecraft and Rockets*, Vol. 29, No. 4, 1992, pp. 556–563.
3) Koshiishi, H., Matsumoto, H., and Goka, T., "Single-Event Upset in Geostationary Transfer Orbit During Solar-Activity Maximum Period Measured by the Tsubasa Satellite," *Advances in Space Research*, Vol. 42, No. 9, 2008, pp. 1500–1503.
4) Wang, Y. and Gurfil, P., "Dynamical Modeling and Lifetime Analysis of Geostationary Transfer Orbits," *Acta Astronautica*, Vol. 128, 2016, pp. 262–276.
5) Wang, Y. and Gurfil, P., "The Role of Solar Apsidal Resonance in the Evolution of Geostationary Transfer Orbits," *Advances in Space Research*, in press, 2017.
6) Morand, V., Le Fèvre, C., Lamy, A., Fraysse, H., and Deleflie, F., "Dynamical Properties of Geostationary Transfer Orbits over Long Time Scales: Consequences for Mission Analysis and Lifetime Estimation," *AIAA/AAS Astrodynamics Specialist Conference*, No. AIAA 2012–4968, Minneapolis, Minnesota, 13–16 August, 2012.
7) Le Fèvre, C., Fraysse, H., Morand, V., Lamy, A., Cazaux, C., Mercier, P., Dental, C., Deleflie, F., and Handschuh, D., "Compliance of Disposal Orbits with the French Space Operations Act: The Good Practices and the STELA Tool," *Acta Astronautica*, Vol. 94, No. 1, 2014, pp. 234–245.
8) Da Costa, B. C., Bernardini, M., Cerf, M., Fessard, M., and Reynaud, S., "Long-Term Semi-Analytical Orbit Propagation Tool for Future European Launchers Design," *AIAA/AAS Astrodynamics Specialist Conference*, No. AIAA 2012–4743, Minneapolis, Minnesota, 13–16 August, 2012.
9) Johnson, N. L., "Space Debris Mitigation Strategies and Practices in Geosynchronous Transfer Orbits," *Advances in Space Research*, Vol. 35, No. 7, 2005, pp. 1328–1334.
10) Siebold, K. and Reynolds, R., "Lifetime Reduction of a Geosyncronous Transfer Orbit with the Help of Lunar-Solar Perturbations," *Advances in Space Research*, Vol. 16, No. 11, 1995, pp. 155–161.
11) Sharma, R., Bandyopadhyay, P., and Adimurthy, V., "Consideration of Lifetime Limitation for Spent Stages in GTO," *Advances in Space Research*, Vol. 34, No. 5, 2004, pp. 1227–1232.
12) Lamy, A., Le Fèvre, C., and Sarli, B., "Analysis of Geostationary Transfer Orbit Long Term Evolution and Lifetime," *Journal of Aerospace Engineering, Sciences and Applications*, Vol. 4, No. 3, 2012, pp. 12–27.
13) Takano, A., Tajima, T., and Kanoh, Y., "Recent Efforts Toward the Minimization of GTO Objects and Its Practices in NASDA," *Acta Astronautica*, Vol. 40, No. 11, 1997, pp. 807–813.
14) Colombo, C., Letizia, F., Alessi, E. M., and Landgraf, M., "End-of-Life Earth Re-Entry for Highly Elliptical Orbits: the INTEGRAL Mission," *The 24th AAS/AIAA Space Flight Mechanics Meeting*, No. AAS 14–156, Santa Fe, New Mexico, 26–30 January, 2014.
15) Armellin, R., San-Juan, J. F., and Lara, M., "End-of-Life Disposal of High Elliptical Orbit Missions: the Case of INTEGRAL," *Advances in Space Research*, Vol. 56, No. 3, 2015, pp. 479–493.